



OPEN

A directed weighted network approach for hazard chain risk assessment including heavy rainfall induced geological disasters and flooding

Jingjing Pei¹, Caiyan Dai¹✉ & Tong Cui²

With the increasing frequency of extreme climatic events in cities, the heavy rainfall–geological hazard–flood urban hazard chain has become more prominent, while traditional single-hazard assessments fail to reveal its systemic transmission mechanisms. This study constructs a hazard chain risk assessment framework based on directed weighted networks to support precise urban disaster identification and control. Using Event Tree Analysis (ETA), 23 key hazard nodes were identified to build a causal loop network, and a Bayesian network was developed to quantify node dependencies. The disaster-bearing body was divided into actual and functional subsystems, and its exposure–vulnerability and disaster resistance capacity were evaluated using an improved Analytic Hierarchy Process and the brittle entropy method. A multi-influence matrix integrating node degree, shortest path, and global influence was designed to calculate the risk weights of 38 nodes and establish the directed weighted network. Applied to Mentougou District, Beijing, the comprehensive hazard chain risk value was calculated as 34.23, and key high-risk nodes were identified. The results show that this model surpasses traditional unweighted or single-hazard methods by enabling dynamic and quantitative evaluation of complex urban hazard chains, offering new insights for enhancing urban resilience and disaster prevention.

Keywords Urban hazard chains, Directed weighted networks, Bayesian networks, Exposure-vulnerability analysis, Hazard chain risk assessment

In recent years, global warming has led to an increasing number of extreme weather events. In urban areas, heavy rainfall often triggers severe secondary disasters. The characteristics of urban systems, combined with prolonged rainfall duration, significantly amplify disaster-induced losses. Due to high population and economic density as well as complex internal interactions, urban disaster systems exhibit features such as risk clustering and nonlinear loss amplification within hazard chains (Shi²¹, Helbing⁷). However, the growing risk of urban hazard chains contrasts with the still underdeveloped emergency management systems. Therefore, this study focuses on hazard chain risk assessment to provide a scientific reference for urban disaster prevention and mitigation.

To date, numerous scholars have proposed models for hazard chain risk assessment. Research in disaster risk management has shifted from single-hazard, linear, and static assessments to the construction of complex network models to reveal the nonlinear and dynamic characteristics of hazard chain risks (Helbing⁷). For example, Menoni proposed the concept of the “disaster loss–damage chain,” which first systematically described disaster coupling effects (Scira Menoni²⁰), and Gill developed a hazard chain analysis framework using a hazard matrix (Gill and Malamud¹⁰). Chen Changkun’s team abstracted the evolution of snow and ice disasters into a network structure and, by combining the risk matrix with the Borda ranking method, achieved quantitative grading of node risks (Chen Changkun and Sun Yunfeng²; Chen Changkun and Xie Mingfeng³). Existing evaluation methods for directed weighted networks mainly identify key nodes by simulating the dynamic transmission of information. However, hazard chain risk assessment should not only focus on node risks within complex network models but also on the risks associated with links between nodes. Current models seldom account for the heterogeneity and directionality of connections, thus failing to fully represent the complex coupling

¹School of Engineering and Technology, China University of Geosciences (Beijing), Beijing 100083, China. ²Huirui Energy Holdings Group Co., Ltd., Ordos 017000, China. ✉email: daicaiyan@email.cugb.edu.cn

effects of hazard chains. For instance, the improved PageRank-based DWCN-NodeRank algorithm by Zhang Kun et al. (Zhang Kun and Li Qibai³²) evaluates node importance in directed weighted networks but cannot simultaneously achieve high accuracy and efficiency. Liu Rui et al. introduced weighted Bayesian networks to reflect the evolution of specific hazard chains through probability transfer mechanisms (Liu¹⁶, Li Ming¹³), yet the transmission direction within the hazard chain remains insufficiently addressed. Although Sanjay Kumar et al.¹² expanded the k-core (ks) decomposition approach to include second-order neighboring nodes using an improved WVoteRank algorithm, potential causal relationships among more distant nodes may still be overlooked. In summary, evaluation of weighted networks should not rely solely on static topology but must also account for differences in information flow caused by varying link weights.

To enhance the modernization of emergency management systems and capabilities, this study analyzes disaster-influencing factors and integrates methods such as Event Tree Analysis (ETA) and Bayesian networks to construct a complex network that incorporates emergency response capacity. The correlations among different disaster events are comprehensively considered, and by quantifying the interaction intensity between nodes, an unweighted structural network is refined into a directed weighted simulation network. While systematically assessing urban hazard chain risks, this study dynamically considers the interactions among multiple factors and develops a more comprehensive evaluation approach. The findings can assist grassroots decision-makers in urban areas facing similar disaster scenarios in identifying critical chain-breaking nodes and improving emergency response actions.

Research methods

Research path

Given the characteristics of heavy rainfall-geological hazard-flooding chain, this study compares existing disaster risk assessment methods. Traditional methods such as the risk matrix and Analytic Hierarchy Process (AHP) are simple and practical, but they rely heavily on subjective expert judgment and static indicator weights, making it difficult to capture the temporal evolution and cascading propagation of disaster processes⁴. Fuzzy comprehensive evaluation and grey system analysis are applicable to uncertainty problems, however, they focus primarily on indicator scoring and classification, failing to reflect inter-hazard dependencies and system feedback mechanisms (Yuxiang Yang, 2025). Machine learning and remote sensing approaches can identify correlations between nodes, but they cannot distinguish causality and often require large datasets (Nikolay Kazanskiy¹⁸). In addition, some studies use single Bayesian networks to assess landslide or flood risk (Zening Wu, 2019); although they address uncertainty, their structures largely depend on expert-defined relationships and lack systematic identification of hazard chain logic and key propagation paths. Thus, current methods exhibit the following limitations: a. They assume disasters as linear and independent events, ignoring coupling and cascading relationships; b. They struggle to simultaneously consider system feedback structures and conditional probability reasoning; c. They have limited ability to identify critical nodes and reveal risk transmission paths.

To address these gaps, this study establishes a comprehensive assessment framework for compound hazard chains based on “Event Tree – Causal Loop Diagram (CLD) – Bayesian Network – AHP and Brittle Entropy – Multi-Influence Matrix.” First, Event Tree Analysis (ETA) is used to trace the evolution paths of storms inducing landslides, debris flows, and flooding, identify key nodes, and construct the temporal logic of the hazard chain. Second, Causal Loop Diagrams from system dynamics are introduced to incorporate positive and negative feedback mechanisms, overcoming the limitations of traditional methods in reflecting nonlinear interactions and self-reinforcing effects²⁴. Compared with studies inferring hazard relationships solely from statistical data, this step provides a structured causal network for Bayesian modeling, reducing subjective bias.

Based on this, a Bayesian network is constructed to model disaster chain reasoning, quantify node states, and assign conditional probabilities. Subsequently, the improved AHP is used to identify key influencing factors of the actual disaster-bearing body from the exposure-vulnerability perspective. The brittle entropy method is applied to evaluate the disaster resilience of functional disaster-bearing subsystems, enabling the construction of an urban vulnerability assessment system. Finally, a multi-influence matrix is used to analyze the driving and dependence degrees among nodes. Combined with the TOPSIS method to determine relative closeness, nodes are ranked and weighted — meaning the results provide not only “risk values” but also “high-sensitivity nodes.”

The following is the technical roadmap of this research (Fig. 1):

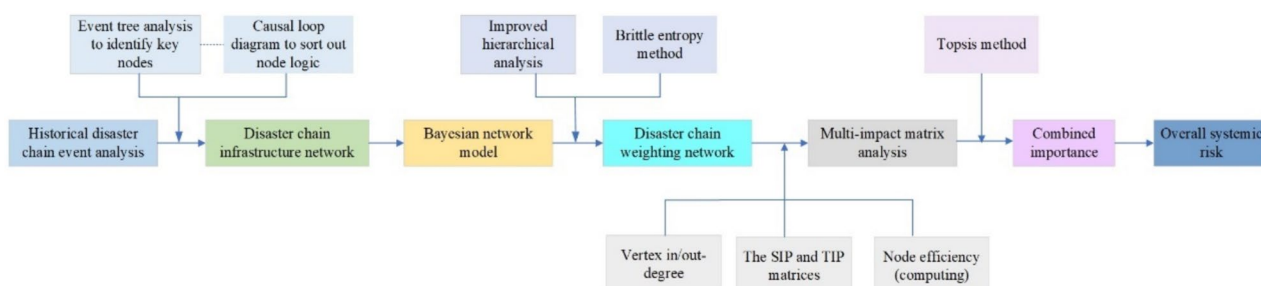
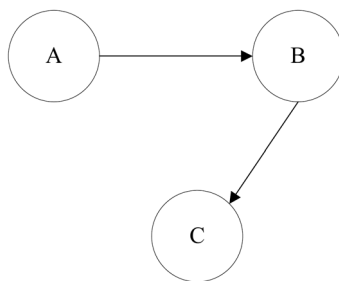


Fig. 1. Research technology roadmap.

**Fig. 2.** Bayesian network schematic.

Event title	Overview
15 July 2006 Heavy Rainfall in Shaoguan	Heavy rainfall triggered torrential mountain floods and widespread inundation; 32 small reservoirs and 1,081 irrigation facilities were damaged; 84 ponds and dams were washed away; 105.2 kms of communication lines were disrupted; three bridges collapsed and 73 sections of road were severed. Floodwaters destroyed 110,000 cubic metres of road foundations and 66.94 kms of road surface
17 May 2010: Heavy Rainfall in Tongren, Guizhou	The heavy rainfall has triggered geological hazards in parts of five counties—Dejiang, Songtao, Yanhe, Shiqian, and Jiangkou—resulting in damage to some crops, collapse of residential buildings, and varying degrees of damage to infrastructure including roads and water conservancy facilities
21 July 2012 Heavy Rainfall in Beijing	Numerous sections of the city's roads, bridges and water conservancy projects sustained damage, with multiple residential buildings collapsing across the municipality and hundreds of vehicles suffering severe losses. Preliminary estimates indicate economic losses approaching ten billion yuan citywide. The disaster resulted in 79 fatalities

Table 1. Major heavy rainfall disaster events in China over a 25-year period (excerpt).

Bayesian network model

A Bayesian network is an extension of Bayesian theory and consists of:

It is represented by a directed acyclic graph. Nodes A, B, and C represent variables, and directed arrows denote the relationships between them (see Fig. 2). Event A is called the parent node, serving as the foundation of the network, and its probability is defined as the prior probability, typically derived from expert knowledge. Event C is the child node, which represents the outcome and directly supports decision-making. Event B is an intermediate node, which can act as the parent of C or the child of A. Directed edges generally point from parent to child nodes. If two nodes are not connected by an arrow, they are conditionally independent.

In the Bayesian network, Event A is defined as the parent node. It forms the basis of the network structure, and its probability is referred to as the prior probability, which is associated with objective laws and is typically derived from expert knowledge. Event C is the child node, representing the final result of Bayesian reasoning and directly serving decision-making needs. Event B is an intermediate node, which may function either as a parent of C (influencing the child node through prior probabilities) or as a child of A (receiving the influence of prior probabilities from the parent node). Directed edges in a Bayesian network generally point from parent nodes to child nodes. If no arrow exists between two nodes, it indicates conditional independence between them.

Each node is associated with a Conditional Probability Table that characterizes its dependency on its parent nodes. Let X be a variable and P_a the set of its parent nodes. Then, the joint probability of all variables in the network can be expressed as:

$$P(X) = \prod_{i=1}^n P(X_i|P_a) \quad (1)$$

Bayesian network model building

Node identification and segmentation

To construct the logical network of the heavy rainfall-geological hazard-flooding chain, this study collected reports of 27 storm-induced disaster events in China over the past 25 years using online news and official databases. These cases were used to comprehensively identify possible secondary hazards triggered by heavy rainfall (selected cases are shown in Table 1). The identification logic here is based on event tree analysis, which analyses the results of subsequent events that may result from the event. For example, take the 6.13 Shenzhen disaster in 2008; the disaster chain can be deduced from the following reports (Fig. 3):

Duration of 10 h, within an hour, Xujiahui area has nearly 120 mm of heavy rainfall, rainfall in some areas of the storm as high as 143 mm, the rainstorm caused, roads are seriously waterlogged, a total of more than 3,000 traffic accidents of various types, rail traffic many times dangerous, flights are delayed.

According to the analysis, the formation of the heavy rainfall-geological hazard-flood disaster chain consists of three components: first, the heavy rainfall, the washout of rainfall and the cumulative effect of rainfall are the key driving factors inducing the disaster chain, and they are the main disaster-causing factors causing the destabilisation of the relatively stable disaster-conceiving environment (Culler⁶; Dalia Kirschbaum⁵; Roland Kaitna¹⁹). For the event of heavy rainfall, the two most important discriminatory factors are the intensity and duration of rainfall, so the two nodes of rainfall intensity and rainfall duration are selected. The combination of

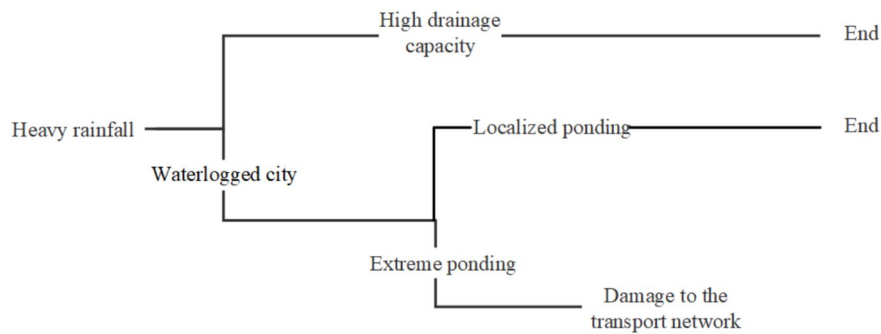


Fig. 3. Example of event tree analysis method.

Number	Node name	Number	Node name
A1	Rainfall intensity	B13	Topographical difference
A2	Rainfall duration	C14	Landslide
B3	Lithological	C15	Debris flow
B4	Geological structure	C16	Debris dammed lake
B5	Slope protection	C17	Flash flood
B6	Gradient	C18	Flooding (return period)
B7	Intensity of anthropogenic activity	C19	Waterlogged
B8	Vegetation (land surface type)	D20	Building collapse
B9	Loose soil	D21	Casualty
B10	Original water system	D22	Crops destroyed
B11	Riverbank dam	D23	City function
B12	Drainage capacity		

Table 2. Key nodes of the heavy rainfall-geological hazard-flooding chain.

heavy rainfall and the other two components can be regarded as two sub-systems, mountainous and urban, so the selection of nodes is also split into two systems, which are identified separately.

For the mountain subsystem, topographic differences and geological formations determine the potential energy of landslide and debris flow hazards. The mountain subsystem provides the main contextual environment for the incubation and development of hazards. The most frequent hazard events within this region include landslides, debris flows and flash floods. Of these, both landslides and debris flows are generally slope geotechnical instability problems and are often interrelated in their genesis (Liu¹⁵). In the whole mountain subsystem, nodes reflecting objective local conditions that affect the probability of disasters other than heavy rainfall should also be included. By analysing the causes of geological hazards such as landslides and mudflows, the influencing factors can be summarised as geological, geomorphological, hydrological and anthropogenic vegetation conditions (Hu⁹). Specific factors may include Lithological, geological structure, slope protection, gradient, intensity of anthropogenic activity, vegetation (land surface type), loose soil, original water system, riverbank dam, and drainage capacity (Thapa²⁶, He¹⁴; Kadirhodjaev, Azam¹¹).

The urban subsystem mainly represents the disaster-bearing body, which is the subject of disaster losses. The main characteristic of this region is the high number of man-made structures. Artificial buildings can be divided into three categories: disaster prevention and mitigation projects, infrastructure to maintain the basic functions of the city, and civil buildings that need to be considered as disaster-bearing bodies. Analysed from the perspective of disaster-bearing bodies, urban disaster-bearing bodies mainly include population, buildings, economy, crops and infrastructure, etc. Among them, the economic loss is usually converted by counting other disaster-bearing bodies (Zhao Axing and Ma Zongjin³³).

Based on the results of the event tree analysis and a review of relevant literature, the following key points have been selected (Table 2):

For all of the above nodes, relationships were identified in groups of two using the Causal Loop Diagram (CLD) in Vensim, usually using arrows marked with '+' and '-' to indicate the relationship between factors. Arrows marked with '+' and '-' are usually used to indicate the relationship between the factors, and the two are considered positively correlated if there is an induced effect. If the high reliability strength of the parent node can inhibit the occurrence of the events of the child node or the occurrence of the events of the parent node can reduce the reliability strength of the child node, the two are considered to be negatively correlated. The causal loop diagram drawn accordingly is shown below (Fig. 4):

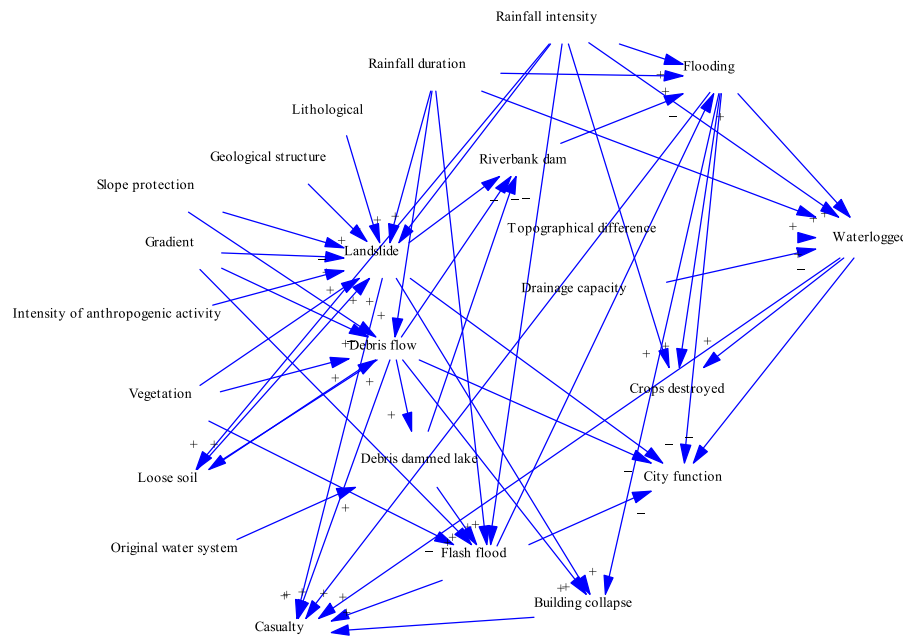


Fig. 4. Causal loop diagram of the heavy rainfall-geological hazard-flooding chain.

Conditional probability learning

The construction of the disaster chain Bayesian network model requires the establishment of a Bayesian network graph, according to which causal inference is applied to achieve probabilistic prediction. In this paper, the Bayesian network is used to reason about the probability of occurrence of each disaster event in Mentougou District, in order to quantitatively describe the process of disaster chain risk formation in the place. Before learning the Bayesian network, it is necessary to clarify the possible states of each node, in the event tree theory, each node has at least two states of 'yes' and 'no'. In order to guarantee the accuracy of the results and clarify the severity of the event, reference to China's National Meteorological Administration, the geological disaster prevention and control engineering industry and some standards in the field of production safety and related literature (Yang Qigui and Zhou Heqing²⁹; Shuai Min²²) for each node is divided into 2–5 different states, which are divided as follows (Table 3):

In this paper, based on past news such as Xinjing Newspaper, National Emergency Broadcasting, Beijing Flood Control Press Conference, Baidu Encyclopedia and other past news, we statistically analysed the summer rainstorms in Beijing over the past 20 years, consulting with experts to determine the status of the intermediate nodes. Arrange and combine the states of the derived base nodes to construct a conditional probability learning database tailored to local conditions in Beijing (Table 4). The model database is characterised by the fact that it is tailored to the realities of Beijing and removes some of the extreme combinations that are beyond the geography of the district, which improves the accuracy and relevance of the model learning and, at the same time, reduces the need for big data.

For the probability of possible induced effects between disaster chains, the Expectation Maximisation (EM) algorithm is applied for parameter learning, and the missing variables are estimated for the incomplete dataset, so as to form a training dataset with no missing data; and then probabilistic statistics for the case of no missing data is applied to obtain the conditional probability parameters, and the approximate infer the likelihood of a disaster chain occurring.

Prior probability analysis

Based on the historical data of Mentougou District, the a priori probability of some nodes in the model is corrected by combining experts' scoring of the status of the local base nodes. Among all the nodes identified, nodes A1-B11 belong to the basic nodes, i.e., nodes whose status can be judged in advance before the occurrence of the event. For this part of the nodes, the collected statistical data of Mentougou District is provided to the risk assessment expert group, and the a priori probability that Mentougou District is in the status of different nodes at present is judged based on the distribution of the scoring interval of the experts or the average of the whole country.

The expert group consisted of eight experts, five of whom were local Beijing scholars engaged in disaster risk assessment research, and three of whom were front-line staff members of the Mentougou District department responsible for emergency response and disaster reduction. Combining the results of learning from the past 20 years of June–August rainstorm disaster cases in Beijing and the scoring opinions of the experts, the a priori probabilities of the new model were determined as follows (Table 5):

Number	Node name	Status value
A1	Rainfall intensity (Rainfall per unit of time /mm/d)	[0~25] / [25~50] / [50~100] / [100~250] / [250~]
A2	Rainfall duration (Duration of rainfall /h)	[0~12] / [12~24] / [24~48] / [48~]
B3	Lithological	Solid / Not solid
B4	Geological structure	Stable / Unstable
B5	Slope protection	Supported / Unsupported
B6	Gradient	Not steep / Steep
B7	Intensity of anthropogenic activity	No mining / light mining / heavy mining
B8	Vegetation (land surface type)	Dense forest / shrubland / grassland / wasteland
B9	Loose soil	Tight / loose
B10	Original water system (River flow /m ³ /s)	[0~200] / [200~1500] / [1500~2500] / [2500~]
B11	Riverbank dam	With / without levee
B12	Drainage capacity	Strong / Weak
B13	Topographical difference (m)	[0~200] / [200~400] / [400~600] / [600~800]
C14	Landslide (Landslide volume /10 ⁴ m ³)	None / [0~10] / [10~100] / [100~1000] / [1000~]
C15	Debris flow (Total cubic metres stacked /10 ⁴ m ³)	None / [0~1] / [1~10] / [10~50] / [50~]
C16	Debris dammed lake (storage capacity /10 ⁴ m ³)	None / [0~100] / [100~1000] / [1000~10000] / [10000~]
C17	Flash flood	None / general flash floods / high sand content flash floods
C18	Flooding (return period)	None / [0~5] / [5~20] / [20~50] / [50~]
C19	Waterlogged	None/general/severe
D20	Building collapse	None/ slightly damaged/ severely damaged
D21	Casualty (Number of casualties/person)	[0~3]/[3~10]/[10~30]/[30~]
D22	Crops destroyed (Affected area /km ²)	None / [0.01~500] / [500~1000] / [1000~1500]
D23	City function	No damage / slight damage / general damage / severe damage

Table 3. Possible states of the nodes of the heavy rainfall-geological hazard-flooding chain and classification criteria.

A1	A2	B3	B4	B5	B6	B7	B8	B9	B10	B11	B12	B13	C14	C15	C16	C17	C18	C19	D20	D21	D22	D23
D	D	B	B	A	B	A	B	B	B	A	A	C	A	C	A	B	C	C	B	C	B	D
B	B	B	B	A	B	A	B	B	B	A	A	C	A	A	A	A	A	A	A	A	A	B
C	C	B	B	A	B	A	B	B	B	A	A	C	B	A	A	A	A	B	A	A	A	B
C	C	B	B	A	B	A	B	B	B	A	B	C	A	A	A	A	A	A	A	A	A	A
B	B	B	B	A	B	A	B	B	B	A	A	C	A	A	A	A	A	B	A	A	A	B

Table 4. Conditional probability database (excerpt).

Number	Node name	Prior probability
A1	Rainfall intensity	0.001 / 0.675 / 0.173 / 0.150 / 0.001
A2	Rainfall duration	0.051 / 0.299 / 0.564 / 0.084
B3	Lithological	0.247 / 0.753
B4	Geological structure	0.614 / 0.386
B5	Slope protection	0.876 / 0.124
B6	Gradient	0.372 / 0.628
B7	Intensity of anthropogenic activity	0.731 / 0.267 / 0.001
B8	Vegetation (land surface type)	0.002 / 0.940 / 0.057 / 0.002
B9	Loose soil	0.324 / 0.676
B10	Original water system (River flow /m ³ /s)	0.001 / 0.996 / 0.002 / 0.001
B11	Riverbank dam	0.949 / 0.051
B12	Drainage capacity	0.736 / 0.264
B13	Topographical difference (m)	0.001 / 0.002 / 0.996 / 0.001

Table 5. Bayesian model prior probabilities for each node.

Simulation results and validation

Combined with the conditional probabilities trained by the EM algorithm, the final model computes the posterior probability of each node in the current situation as follows (Fig. 5):

Verifying the accuracy of probabilistic parameters of Bayesian networks based on Genie sensitivity. The definition of sensitivity essentially reflects the strength of the influence of the changes of the higher-level nodes on the lower-level nodes, and the distribution of sensitivity and the distribution of the influence weights of the nodes are highly convergent for the network in which multiple nodes jointly determine the state of the lower-level nodes. Therefore, within this subsystem, the normalisation result of sensitivity is used as the main basis for weight distribution. The link edges A1-C14 are used to denote the sensitivity of node A1 to have influence on node C14, and the sensitivity of each initial node to the intermediate nodes and each intermediate node to the final node is analysed by Genie software, with a variation value of 10%, and the final results are as follows (Table 6):

Disaster resilience analysis and risk assessment

Influencing factors analyzing

Traditional Bayesian network-based disaster chain analysis mainly focuses on the probability of disaster occurrence and the formation process of disasters, but it is insufficient for analysing the correlation between disaster bearers. By analysing the influencing factors of the disaster-bearing part of the Bayesian network, it helps to analyse its internal correlation and enhance the integrity of the risk assessment model. In this paper, the hazard-bearers are mainly considered from the perspectives of population, buildings, crops and basic functions of the city. By splitting disaster-bearing bodies into actual disaster-bearing bodies and functional disaster-bearing bodies, and determining the link side weights using different methods respectively, the differences of urban disaster-bearing bodies are expressed from three perspectives of exposure, vulnerability and resilience, with the intention of analysing the full model of influencing factors affecting the risk-resistant capacity of disaster-bearing bodies.

Exposure performance is the volume of disaster-bearing bodies affected by disasters and accidents, and the number of disaster-bearing bodies as well as their spatial distribution characteristics can reflect the exposure of the urban system more intuitively. In this paper, three indicators, namely, average population density, urban area, and GDP of agricultural products, are mainly selected as the basis indicators for assessing the exposure of urban systems.

The first aspect of vulnerability is for the disaster-bearing population, and the most frequently used evaluation indicator is population density as the main evaluation indicator (Wu Zongzhi²⁸). In the disaster chain of heavy

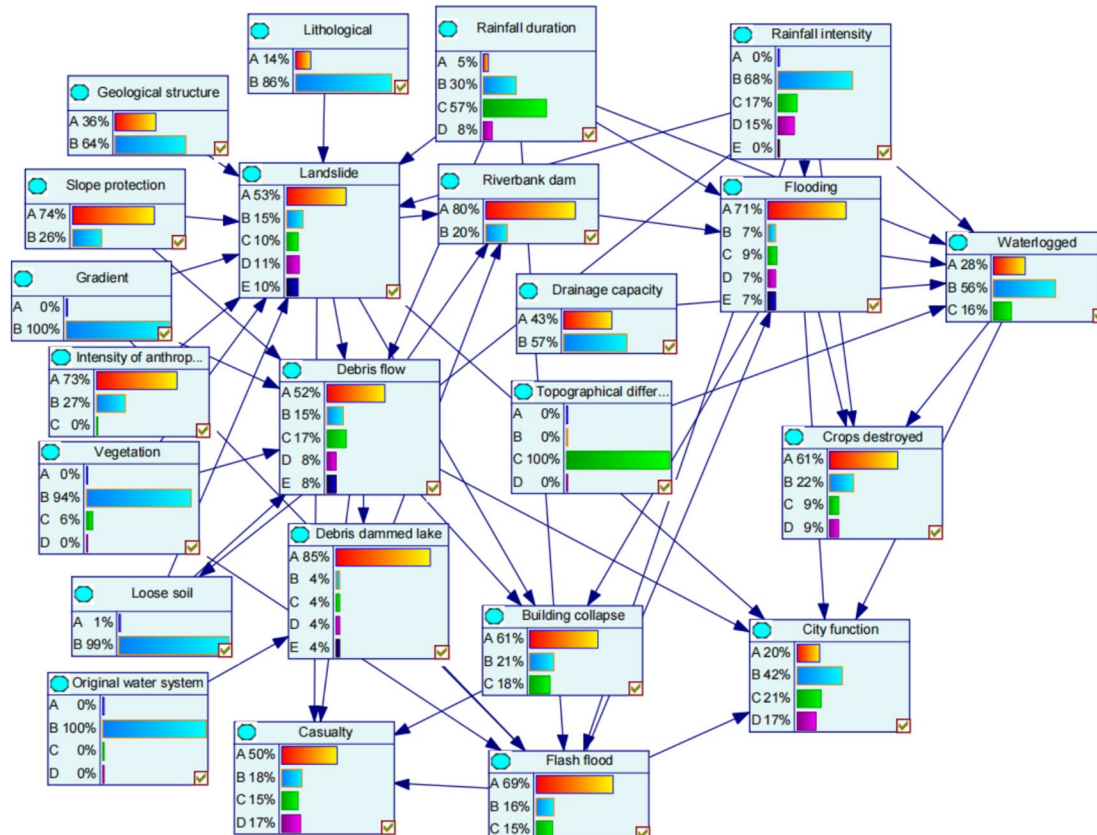


Fig. 5. Bayesian probabilistic model simulation results.

Relevant node	Sensitivity	Relevant node	Sensitivity
A1-C14	0.329	A2-C18	0.513
A2-C14	0.329	B11-C18	0.26
B3-C14	0.298	C17-C18	0.123
B4-C14	0.045	A1-C19	0.378
B5-C14	0.28	A2-C19	0.263
B6-C14	0.33	B12-C19	0.164
B7-C14	0.33	B13-C19	0.224
B8-C14	0.349	C18-C19	0.1
B9-C14	0.294	C14-D20	0.053
A2-C15	0.32	C15-D20	0.213
B5-C15	0.21	C18-D20	0.11
B6-C15	0.32	C14-D21	0.041
B8-C15	0.32	C15-D21	0.14
B9-C15	0.252	C17-D21	0.115
C14-C15	0.05	D20-D21	0.233
B10-C16	0.655	A1-D22	0.526
C15-C16	0.214	C18-D22	0.131
A1-C17	0.358	C19-D22	0.121
A2-C17	0.359	C14-D23	0.028
B6-C17	0.358	C15-D23	0.092
B8-C17	0.358	C17-D23	0.104
C16-C17	0.238	C18-D23	0.078
A1-C18	0.507	C19-D23	0.069

Table 6. Calculation of the sensitivity of each node of the Bayesian model.

rainfall-geological hazards-flooding, the tests suffered by the disaster-affected population can be divided into two categories, namely, the ability to cope with sudden-onset disasters and the ability to tolerate prolonged periods of time in a disaster environment. The former is usually associated with the self-rescue technical capacity of the same population, while the latter is more closely related to the average physical capacity of the local population. The definitions and quantitative methods of the selected indicators are given below:

1. Self-help technology index $P_{vul(edu)}$

$$P_{vul(edu)} = \frac{POP_{edu}}{POP} \times 100\% \quad (2)$$

where: $P_{vul(edu)}$ is the urban self-rescue technology index; POP_{edu} is the number of people with disaster emergency self-rescue capability, and the ratio of people with post-secondary education is used to characterise the self-rescue technology index; and POP is the total urban population.

2. Urban population fitness index $P_{vul(age)}$

$$P_{vul(age)} = 1 - \frac{POP_{elder} + POP_{child}}{POP} \times 100\% \quad (3)$$

where: $P_{vul(age)}$ is the physical fitness index of the urban population; POP_{elder} is the number of elderly (≥ 65) population in the city; POP_{child} is the number of children (≤ 14) population within the city; and POP is the total urban population. The above parameters can be obtained from the demographic statistics of Mentougou District.

Secondly, for the disaster-bearing body of buildings, in the disaster chain of heavy rainfall-geological hazards-flooding, buildings will be subjected to forces such as immersion, scouring and wind blowing, etc. Currently, the research on the seismic damage sensitivity of buildings is more mature, and it is generally measured by the building structural index, which characterises the structural damage sensitivity of the building, and the time-of-use index, which affects the damage sensitivity of the building because of the time of use. For flooding, the local surface runoff coefficient is also taken into account to measure the water retention capacity of local buildings. The definitions and quantitative methods of the selected indicators are given below:

3. Building structure index

$$H_{\text{vul(str)}} = \sum_{i=1}^4 \left(\frac{S_i}{S} \right) VID_i \quad (4)$$

where: i is the category of housing structure, defining the common domestic 1–4 categories of building structure in the order of earth and wood structure, brick and wood structure, brick-concrete structure, steel-concrete structure; S_i is the corresponding structure of the housing area (number of rooms); S is the total area of the housing area in the region (the total number of rooms); VID_i on behalf of the i th category of housing relative to the average rate of loss of a particular type of disaster, (1–4 loss rate reference(Zhou³⁴) in architecture design.).

4. Building depreciation rate.

The longer a house is in use, the less able it is to withstand external shocks, the more sensitive it is to various types of disasters, and the more likely it is to suffer damage. Setting the parameter of depreciation rate quantifies its capacity in the interval from 0 to 1. The indicator is defined as follows:

$$H_{\text{vul(T)}} = \frac{\sum_{i=1}^n \frac{T_u}{T_{de}}}{n} \quad (5)$$

where: T_u and T_{de} represent the number of years the building has been in use and the design life, respectively; when the number of years the building has been in use, T_u , exceeds the design life, T_{de} , the depreciation rate is set to be 1. n represents the number of building samples investigated.

5. Weighted pavement runoff coefficient.

Based on the runoff coefficients of different road surfaces in the ‘Calculation Standards for Stormwater Runoff in Planning and Design of Urban Stormwater Systems’, and using the approximate proportions of the different land uses in the area under study as the weightings, the composite runoff coefficient of the area will be calculated, which will serve as a quantitative indicator for evaluating the drainage capacity of its road surfaces.

6. Recombination rate during the heavy rainfall fruiting period.

For the crop disaster-bearing body, the first consideration of its exposure to agricultural GDP ratio as a measure of indicators, followed by consideration of the planting of different categories of crops and their growth cycle, the Beijing Mentougou District, the main agricultural products Beijing White Pear as an example, the summer June–August pear tree in the stage of the just hanging fruit, there are often for the ripening of the fruit by the impact of rainstorms were knocked down. Assuming that the date of pear tree fruit in June–August in line with the standard normal distribution:

$$f(x) = \frac{1}{11.5 \times \sqrt{2\pi}} e^{-\frac{(x-46)^2}{264.5}} \quad (6)$$

where the mathematical expectation μ is half the number of days in June–August, i.e. 46. its left and right 4σ intervals, i.e. 46 days contains 99.99% probability. The percentage of pear trees affected during the duration of the rainstorm was used as a quantitative indicator of crop growth cycle factors.

For the urban functional disaster-bearing body, with reference to the division of urban lifeline projects, the system that guarantees the operation of the basic functions of the city is divided into six sub-systems, namely, power, gas storage, water, underground pipelines, transport and communications: the power system mainly represents the power generation capacity of the power plant and the supporting transmission capacity; gas represents the city's reserves of natural gas, oil, petrol and other energy sources. The water source mainly represents the water purification capacity of the waterworks and the ability to distribute the required industrial water to key nodes. Underground pipelines represent the ability to transport clean water or fuel to various nodes in the city. Transportation represents the city's ability to move various resources through various vehicles, aircraft, ferries, and other modes of transport. Communication systems represent the ability of the city to control and exchange real-time information.

The Indices for evaluating the exposure vulnerability of urban disaster-bearing bodies are shown in the table below (Table 7):

Weighting allocation

The weights of the exposure-vulnerability indicator

The weights of the exposure-vulnerability disaster-bearing body indices were determined by the hierarchical analysis method. The weight allocation method given in Sect. 4.2 was also used to integrate the experts' opinions

Goal layer	Criteria layer	Sub-criteria layer	Alternatives layer
Vulnerability assessment of urban disaster-bearing bodies	Building exposure-vulnerability (J)	Building exposure	Urban area (H_e)
		Building vulnerability	Infrastructure strength ($H_{vul(str)}$)
			Degree of building ageing ($H_{vul(T)}$)
			Building hydrophobicity (H_h)
	Personnel exposure-vulnerability (R)	Personnel exposure	Population density (P_e)
		Personnel vulnerability	Personnel emergency response capacity ($P_{vul(edu)}$)
			Personnel tolerance ($P_{vul(age)}$)
	Crop exposure-vulnerability (N)	Crop exposure	GDP of agricultural products (N_e)
		Crop vulnerability	Crop growth cycle (N_c)

Table 7. Index system for evaluating the exposure vulnerability of disaster-bearing bodies.

Classify	Eigenvector	Weight value	Maximum eigenvalue	CI value
Urban area	1.253	31.333%	4.123	0.041
Infrastructure strength	1.911	47.770%		
Degree of building ageing	0.648	16.210%		
Building hydrophobicity	0.187	4.687%		

Table 8. Exposure-vulnerability indices weights for building disaster-bearing bodies.

Classify	Eigenvector	Weight value	Maximum eigenvalue	CI value
Population density	2.089	69.646%	3.124	0.062
Personnel tolerance	0.703	23.422%		
Personnel emergency response capacity	0.208	6.932%		

Table 9. Population exposure-vulnerability indicator weights.

Classify	Eigenvector	Weight value	Maximum eigenvalue	CI value
GDP of agricultural products	1.676	83.780%	2.000	0.000
Crop growth cycle	0.324	16.220%		

Table 10. Exposure-vulnerability indicator weights for crop disaster-bearing bodies.

after 8 experts' deliberations. Based on the sum-product approximation, and after passing the consistency test, the weights of the indicators were found as follows (Table 8; Table 9; Table 10):

Vulnerability weights for urban functions

According to the idea of vulnerability theory, taking the six subsystems of electricity, gas storage, water source, underground pipeline, transport and communication as examples, on the basis of the qualitative analysis of the interactions of lifeline subsystems (five ways of interactions among functions of the city include: interdependence, mutual proximity, mutual substitution, and assistance in repairing) (Liu¹⁴), the entropy theory is adopted to quantify the degree of uncertain interactions. Thus, the brittle correlations between urban lifeline systems are analysed and combined with the disaster damage sensitivity of single-function lifeline systems, so as to evaluate the disaster damage sensitivity of urban lifeline systems as a whole.

Firstly, the association Boolean matrix is constructed and summed to get the composite matrix, and each column of the composite matrix is summed to get the association of each sub-system affected by other sub-systems:

Electricity=10, Gas Storage=7, Water source=7, Underground Pipeline=10, Transport=11, Communication=5.

Of the four types of relationship, neighbourhood influence can be characterised as brittle homogeneity, substitution can be characterised as brittle opposition; and reliance influence and repair influence can be characterised as brittle fluctuation.

Electricity: $P_a=1/10, P_b=1/10, P_c=8/10, H_a=0.230, H_b=0.230, H_c=0.179; \omega_a=0.480, \omega_b=0.613, \omega_c=0.65; H_d=0.368.$

Gas Storage: $P_a=0, P_b=1/7, P_c=6/7; H_a=0, H_b=0.278, H_c=0.132; \omega_a=0, \omega_b=0.653, \omega_c=0.603; H_{ch}=0.261.$

Water source: $P_a=1/7, P_b=0, P_c=6/7; H_a=0.278, H_b=0, H_c=0.132; \omega_a=0.527, \omega_b=0, \omega_c=0.603; H_s=0.226$.
 Underground Pipeline: $P_a=2/10, P_b=1/10, P_c=7/10; H_a=0.322, H_b=230, H_c=0.250; \omega_a=0.567, \omega_b=0.613, \omega_c=0.707; H_g=0.500$.
 Transport: $P_a=1/11, P_b=2/11, P_c=8/11; H_a=0.218, H_b=0.310, H_c=0.232; \omega_a=0.467, \omega_b=0.677, \omega_c=0.694; H_j=0.472$.
 Communication: $P_a=1/5, P_b=1/5, P_c=3/5; H_a=0.322, H_b=0.322, H_c=0.306; \omega_a=0.567, \omega_b=0.685, \omega_c=0.744; H_t=0.631$.

Construction of weighted network mode

After Genie's sensitivity analysis between nodes, the structure is simplified into a unidirectional network with initial nodes to intermediate nodes and intermediate nodes to final nodes. Then the refinement of the overall network is completed by constructing the exposure-vulnerability indicator factor evaluation model of the disaster-bearing body, and its overall network node diagram is as follows (Fig. 6):

In order to rationally assign individual link side weights, the weights between subsystems derived from different methods need to be harmonised. Firstly, a hierarchical analysis of hazard and exposure vulnerability is conducted to derive the weight share of the two larger dimensions:

According to the expert rating opinion and combining the results of most scholars (Hu Haibo⁸; Bai Wanping¹) who have conducted PHA analyses for urban disaster risks, the ratio of hazard and exposure-vulnerability is roughly 0.607:0.383.

Max-min normalisation is performed to normalise the network weights in the range [0–1]. The formula is as follows:

$$\omega_i = \frac{x_i - x_{min}}{x_{max} - x_{min}} \quad (7)$$

where ω_i is the link edge weight, x_i is the sensitivity of link edge i , and x_{max} and x_{min} are the maximum and minimum values in the full sample. When $x_i=x_{min}$, it is set as a very small positive number with a value slightly greater than $0 (1 \times 10^{-3})$. The final results are as follows (Table 11):

In order to comprehensively consider the influence of other nodes in the system when calculating the node importance degree, this paper refers to the directed weighted network method based on multiple influence matrix proposed by Wang Yu et al. (Wang Yu and Guo Jinli²⁷) to evaluate the important nodes of the network constructed in this paper. According to the node degree calculation, node network efficiency calculation, multiple influence matrix construction, the importance degree of node i is defined in the formula to calculate

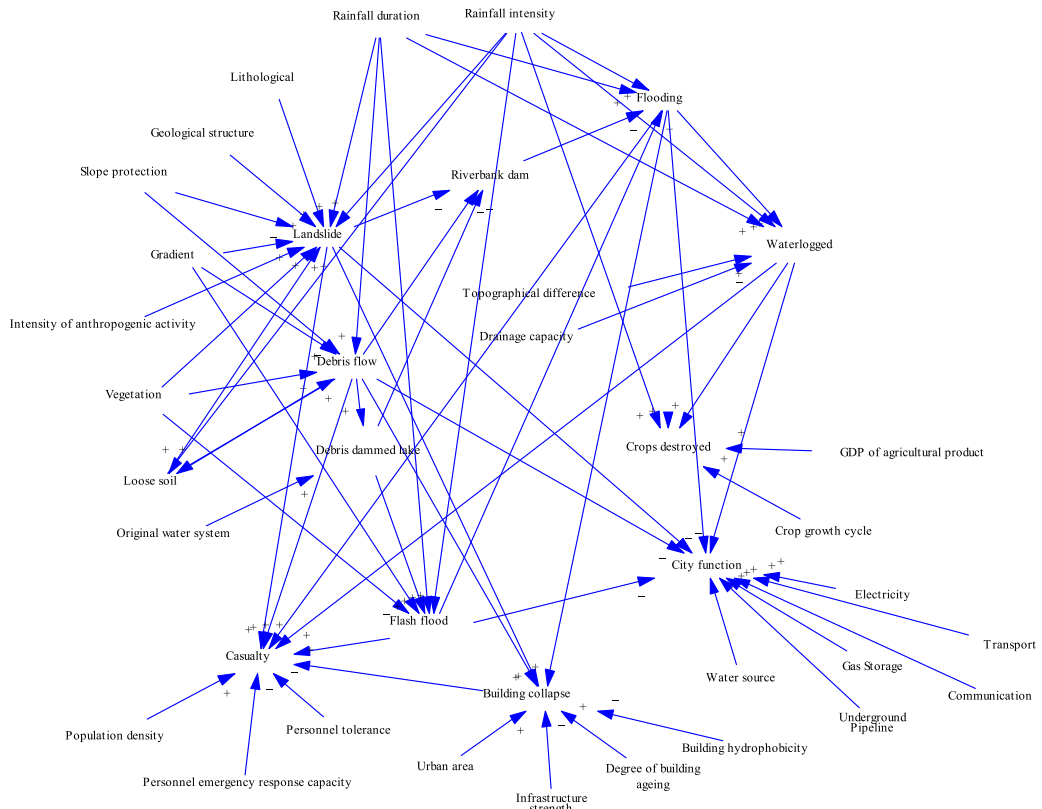


Fig. 6. Integrated logic diagram of the storm-geological-hazard-flooding chain system.

Link side name	Weight	Link side name	Weight	Link side name	Weight
A1-C14	0.4801	C16-C17	0.3349	C15-D23	0.1021
A2-C14	0.4801	A1-C18	0.7640	C17-D23	0.1212
B3-C14	0.4306	A2-C18	0.7735	C18-D23	0.0797
B4-C14	0.0271	B11-C18	0.3700	C19-D23	0.0654
B5-C14	0.4019	C17-C18	0.1515	J1-D20	0.2703
B6-C14	0.4817	A1-C19	0.5582	J2-D20	0.4364
B7-C14	0.4817	A2-C19	0.3748	J3-D20	0.1184
B8-C14	0.5120	B12-C19	0.2169	J4-D20	0.0026
B9-C14	0.4242	B13-C19	0.3126	R1-D21	0.6558
A2-C15	0.4657	C18-C19	0.1148	R2-D21	0.1908
B5-C15	0.2903	C14-D20	0.0399	R3-D21	0.0248
B6-C15	0.4657	C15-D20	0.2951	N1-D22	0.7987
B8-C15	0.4657	C18-D20	0.1308	N2-D22	0.1184
B9-C15	0.3573	C14-D21	0.0207	G1-D23	0.3257
C14-C15	0.0351	C15-D21	0.1786	G2-D23	0.2180
B10-C16	1.0000	C17-D21	0.1388	G3-D23	0.1828
C15-C16	0.2967	D20-D21	0.3270	G4-D23	0.4585
A1-C17	0.5263	A1-D22	0.7943	G5-D23	0.4303
A2-C17	0.5279	C18-D22	0.1643	G6-D23	0.5903
B6-C17	0.5263	C19-D22	0.1483		
B8-C17	0.5263	C14-D23	0.001		

Table 11. Systematic link side weights for the storm-geological-flood hazard chain.

the importance degree of each node, and the calculation results and the final ranking are shown in the following table (Table 12):

The relative posting progress derived based on topsis is normalised so that the sum of all node weights is equal to 10, which is satisfied:

$$\sum_{i=1}^n w_i = 10 \quad (8)$$

The node weights obtained at this point are regarded as the weights of the individual node risks in this model with respect to the total system risk.

Case study

The realistic risk of Beijing Mentougou District is calculated by quantifying the realistic risk value of each node. Among them, for the disaster-bearing environment and disaster nodes, the risk value can be derived from the Bayesian model results by calculating the expected value. For the disaster-bearing body attribute node, it needs to be quantified based on the actual data.

For the population, buildings and agriculture in Mentougou District, reference is made to the Mentougou District 2022 National Economic and Social Development Statistical Bulletin, the 2021 Mentougou District Statistical Yearbook, the Seventh National Population Census Bulletin of Mentougou District, Beijing Municipal Statistical Yearbook, as well as the Outline of the Fourteenth Five-Year Plan for the National Economic and Social Development of the Mentougou District and the Visionary Objectives of the Mentougou District for the Year 2035. For the damage to the basic urban functions of Mentougou District, reference is made to news reports on torrential rains in Beijing over the years, mainly from People's Daily Online, Xinhua Net, and Netease News. Based on the calculation of the base risk value for each node is determined in the table below (Table 13):

The basic risk value of each node was combined with its corresponding weight, and overall risk was classified into four levels within the value range of 0–100 (see Table 14). The final result shows that the comprehensive risk value of the heavy rainfall-geological hazard-flooding chain in Mentougou District is 34.23, indicating a “medium to moderately high risk zone”.

Based on the weighted risk values of each node, this study calculated risk values for three types of hazard chains: a. heavy rainfall-geological hazard chain b. heavy rainfall-flooding chain c. heavy rainfall-geological hazard-flooding chain. The results are shown in Table 15.

The findings indicate that the compound hazard chain (34.23) presents a higher risk than either single hazard chain, implying that in mountainous urban environments, if geological hazards and flooding evolve in a cascading manner under heavy rainfall, their impacts may be superimposed or even amplified. The risk of the single heavy rainfall-geological hazard chain (21.47) is relatively low and spatially confined to localized slope failures such as landslides or collapses. The heavy rainfall-flooding chain shows a slightly higher risk (27.65), as it is controlled by drainage capacity and river convergence conditions, resulting in more regional and burst-type impacts.

Node name	S_i^c	$D_{i, \ell}$	Relative proximity	Order of importance	Weight
Rainfall intensity	2.1860	0	0.933	1	1.0461
Rainfall duration	1.7249	0	0.78	2	0.8745
Lithological	0.3014	0	0.137	22	0.1536
Geological structure	0.0190	0	0.008	36	0.0090
Slope protection	0.4845	0	0.22	15	0.2467
Gradient	1.0316	0	0.469	6	0.5258
Intensity of anthropogenic activity	0.3372	0	0.153	20	0.1715
Vegetation (land surface type)	1.0528	0	0.479	5	0.5371
Loose soil	0.5471	0	0.249	14	0.2792
Original water system	0.7000	0	0.318	10	0.3565
Riverbank dam	0.2590	0	0.117	24	0.1312
Drainage capacity	0.1518	0	0.068	30	0.0762
Topographical difference	0.2188	0	0.099	27	0.1110
Landslide	1.1829	0.0411	0.539	4	0.6043
Debris flow	1.2347	0.1570	0.566	3	0.6346
Debris dammed lake	0.6234	0.1434	0.29	11	0.3251
Flash flood	1.0206	0.0911	0.467	7	0.5236
Flooding	0.9604	0.1323	0.441	8	0.4945
Waterlogged	0.5754	0.1217	0.267	12	0.2994
Building collapse	0.5798	0.0808	0.266	13	0.2982
Casualty	0.4610	0.0861	0.213	16	0.2388
Crops destroyed	0.4212	0.0713	0.194	18	0.2175
City function	0.7722	0.0753	0.353	9	0.3958
Urban area	0.1892	0	0.086	28	0.0964
Infrastructure strength	0.2188	0	0.099	26	0.1110
Degree of building ageing	0.0829	0	0.037	35	0.0415
Building hydrophobicity	0.0018	0	0.001	38	0.0011
Population density	0.4591	0	0.209	17	0.2343
Personnel emergency response capacity	0.1336	0	0.06	31	0.0673
Personnel tolerance	0.0174	0	0.007	37	0.0078
GDP of agricultural product	0.1250	0	0.056	33	0.0628
Crop growth cycle	0.0829	0	0.037	34	0.0415
Electricity	0.2280	0	0.103	25	0.1155
Gas Storage	0.1526	0	0.069	29	0.0774
Water source	0.1280	0	0.058	32	0.0650
Underground Pipeline	0.3210	0	0.146	21	0.1637
Transport	0.3012	0	0.137	23	0.1536
Communication	0.4132	0	0.188	19	0.2108

Table 12. Relative proximity of nodes and calculated values of weights.

Conclusions

The current risk situation in China is summarised as with global warming and the continuous advancement of China's industrialisation and urbanisation, extreme weather tends to be stronger, heavier and more frequent, bringing great negative impacts to urban society. In view of this, it is of great practical significance to study the risk of heavy rainfall disaster and its derived disaster chain, with large cities as the main disaster-bearing body. The conclusions of this paper are as follows:

Based on the cases of severe rainstorm disasters in various provinces of China in the past 25 years, the key nodes of the disaster chain propagation were systematically identified and analysed in terms of causative relationships through the event tree method. And by analysing the definitions in disaster science, the disaster event is split into three levels of disaster-conceiving environment, disaster-causing factor and disaster-bearing body, and a logical network of heavy rainfall-geological disaster-flood disaster chain containing three levels and a total of 23 nodes is constructed.

Combined with the risk assessment method, the traditional unweighted complex network of structural importance analysis of the hazard chain based only on the induced relationship was deepened into a directed weighted network combining expert experience, historical probability, vulnerability and other multi-factors. Specific methods used Bayesian probability model, hierarchical analysis and fragility entropy to quantify the importance of each influencing factor in terms of hazard, vulnerability and system resilience, respectively.

Node name	Base risk value	Node name	Base risk value
Rainfall intensity	4.925	Building collapse	3.905
Rainfall duration	4.31	Casualty	3.725
Lithological	6.8	Crops destroyed	2.938
Geological structure	5.7	City function	4.625
Slope protection	3.8	Urban area	9.5
Gradient	7.5	Infrastructure strength	1.075
Intensity of anthropogenic activity	2.945	Degree of building ageing	1
Vegetation (land surface type)	3.9	Building hydrophobicity	7.247
Loose soil	7.45	Population density	9.5
Original water system	3.75	Personnel emergency response capacity	1.917
Riverbank dam	3.5	Personnel tolerance	2.62
Drainage capacity	5.35	GDP of agricultural products	0.02
Topographical difference	6.25	Crop growth cycle	8.9
Landslide	3.15	Electricity	2.216
Debris flow	3.1	Gas Storage	2.018
Debris dammed lake	1.81	Water source	1.455
Flash flood	3.535	Underground Pipeline	1.606
Flooding	2.49	Transport	4.375
Waterlogged	5	Communication	2.125

Table 13. Base risk values for each node of the heavy rainfall-geological hazard-flooding chain.

Risk value R	Risk level	Meaning
0–20	Low	Low probability of occurrence and limited losses
20–40	Medium	There is a possibility of chain-reaction triggering, with localised high-risk areas
40–60	High	Prioritise defence and monitoring
> 60	Extremely high	Prone to triggering a chain of disasters and causing severe losses

Table 14. Risk level classification.

Hazard chain type	Risk value R	Key affected segments	Characterisation analysis
Heavy rainfall-geological hazard chain	21.47	Landslide, debris flow	Spatially dispersed distribution, with localised impact
Heavy rainfall-flooding chain	27.65	River confluence, urban drainage congestion	The impact is concentrated in river valleys and low-lying areas within urban districts
Heavy rainfall-geological hazard-flooding chain	34.23	Landslides blocking valleys and gorges, and the breach of earthen dams causing floods	The cumulative amplification effect is pronounced, exhibiting a chain-like progression

Table 15. Risk values for the heavy rainfall hazard chain.

Using the multiple influence matrix algorithm and TOPSIS algorithm to rank the importance of nodes and assign weights based on the propagation efficiency of a forward-weighted network with a storm-geological-hazard-flood hazard chain as an example, we identify that the high risk in the propagation of the chain mainly comes from the intensity of rainfall, the topographic difference within the area and the excessive population size. Finally, a risk assessment method for disaster chains in directed weighted networks with both spatial topology and temporal evolutionary dynamics is developed.

Discussion

The research discusses the results of the risk assessment. From the baseline risk values across various nodes, it is evident that exposure nodes exhibit significantly higher risk values. This indirectly reflects that the highly concentrated population and economic infrastructure in the Beijing region, coupled with its role as the capital, are the primary reasons why the risk of heavy rainfall disasters in this area receives such high priority.

The next category of high-risk nodes pertains to natural environmental factors such as topography, slope gradient, rock composition, and geological structures. This indicates that Mentougou District possesses unfavourable geographical conditions, with its natural environment inherently predisposing it to elevated risks of geological hazards. Furthermore, owing to these geographical constraints, urban development is concentrated in low-lying, flat terrain with extensive paved surfaces, resulting in a significantly heightened probability of urban

flooding. Next is the influence of rainfall patterns. Due to the surrounding mountainous terrain, precipitation is highly concentrated both temporally and spatially, resulting in a greater likelihood of torrential downpours.

Despite adverse natural conditions, the built infrastructure of Mentougou District is relatively well developed, with substantial governmental investment in disaster prevention, mitigation, and ecological restoration. This ensures that urban emergency functions remain operational during heavy rainfall events. From the perspective of weighted risk values, although the long-term expected risk derived from historical rainfall data is not high, rainfall contributes the largest proportion, and the strong interannual variability of precipitation in Mentougou makes high-risk years more likely. Besides rainfall, high-risk factors include slope gradient, loose soil, and vegetation cover, indicating that soil erosion control and ecosystem restoration are essential for regional safety. In addition, accelerating the development of new urban centers and relocation of residents currently remains an effective strategy for reducing regional risk, and its benefits outweigh the potential increase in urban flooding or management challenges caused by urban expansion.

Urban heavy rainfall disasters are highly complex systems with significant uncertainty and blurred subsystem boundaries. To accurately quantify the risks of both nodes and edges within the hazard chain network, this study adopted multiple weighting methods, which inevitably increased the methodological complexity. Furthermore, the classification of several node states lacks refined criteria, introducing subjectivity and possibly affecting model accuracy.

Although this study refined the disaster chain into a directed weighted network through an indicator-based approach, limitations remain in weight determination due to constraints in time and experience. Future research may focus on: Expanding the Bayesian network database by collecting more disaster cases, refining network structure, and extending the temporal scale of the model; Conducting field surveys to increase spatial resolution by dividing disaster-bearing bodies into grid units, thereby producing more practical urban disaster risk maps; Developing more robust mathematical models, or refining scoring dimensions, to minimize subjectivity within a reasonable range.

Data availability

The datasets used and/or analysed during the current study available from the corresponding author on reasonable request.

Received: 29 August 2025; Accepted: 11 December 2025

Published online: 06 January 2026

References

1. Wanping, B., Yudong, Y. & Zhengzhao, Li. On constructing urban waterlogging risk assessment system in Changzhou. *J. Changzhou Inst. Technol.* **28**(04), 16–20 (2015).
2. Changkun, C., Yunfeng, S. & Zhi, Li. Characteristic analysis of evolution and derivation chain of risk events caused by snow and ice disasters. *J. Catastrophol.* **24**(01), 18–21 (2009).
3. Changkun, C., Mingfeng, X. & Dongyue, Z. Research on quantitative analysis method of disaster evolution network based on risk Matri. *J. Catastrophol.* **37**(01), 13–17 (2022).
4. Cox, L. A. What's wrong with risk matrices?. *Risk Anal.* **28**(2), 497–512. <https://doi.org/10.1111/j.1539-6924.2008.01030.x> (2008).
5. Dalia Kirschbaum, C. et al. The state of remote sensing capabilities of cascading hazards over high Mountain Asia. *Front. Earth Sci.* <https://doi.org/10.3389/feart.2019.00197> (2019).
6. Culler, E. S. et al. A multi-sensor evaluation of precipitation uncertainty for landslide-triggering storm events. *Hydro. Process.* **35**(7), 14260. <https://doi.org/10.1002/hyp.14260> (2021).
7. Dirk, H. Globally networked risks and how to respond. *Nature* **497**, 7447. <https://doi.org/10.1038/nature12047> (2013).
8. Haibo, Hu., Chunyi, X. & Lishang, Z. The pre-event risk assessment of Beijing urban flood. *J. Appl. Meteorol. Sci.* **24**(01), 99–108 (2013).
9. Hu Haopeng. Researches on Debris Flow Hazards Evaluation Indexes System and Method in Beijing [Master's thesis]. China University of Geosciences (Beijing) (2007).
10. Gill, J. C. & Malamud, B. D. Hazard interactions and interaction networks (cascades) with in multi-hazard methodologies. *Earth Syst. Dyn. Discuss.* <https://doi.org/10.5194/esd-7-659-2016> (2016).
11. Kadirhodjaev, et al. Analysis of the relationships between topographic factors and landslide occurrence and their application to landslide susceptibility mapping: a case study of Mingchukur Uzbekistan. *Geosci. J.* **22**(6), 1053–1067. <https://doi.org/10.1007/s12303-018-0052-x> (2018).
12. Kumar, S. & Panda, A. Identifying influential nodes in weighted complex networks using an improved WVoteRank approach. *Appl. Intell.* **52**(2), 1838–1852. <https://doi.org/10.1007/s10489-021-02403-5> (2022).
13. Li Ming;Zhang Ren;Hong Mei. Marine disaster risk assessment based on weighted Bayesian Network. *Mar. Sci. Bull.* **37**(02), 121–128 (2018).
14. Liu Aihua. Research on the Dynamics Evolution Model of Urban Disaster Chain and the Risk Assessment Method of Disaster Chain [PhD thesis]. Central South University (2013).
15. Chuanzheng, L. Genetic types of landslide and debris flow disasters in China. *Geol. Rev* **60**(04), 858–868. <https://doi.org/10.16509/j.georeview.2014.04.017> (2014).
16. Liu Rui. A Study on Modeling of Flood Risk Evaluation Based on Bayesian Networks [PhD thesis]. East China Normal University (2016).
17. He, N. et al. Characteristics of debris flow development in Daxilada watershed and its hazard analysis on Lexi Expressway. *Sci. Reports* **14**(1), 22397. <https://doi.org/10.1038/s41598-024-73305-y> (2024).
18. Kazanskiy, N., Khabibullin, R., Nikonorov, A. & Khonina, S. A comprehensive review of remote sensing and artificial intelligence integration: Advances, applications, and challenges. *Sensors* **25**(19), 5965. <https://doi.org/10.3390/s25195965> (2025).
19. Kaitna, R. et al. Climate induced increase in frequency and area affected by critical rainfall conditions triggering debris flows in Austria. *Commun. Earth Environ.* <https://doi.org/10.1038/s43247-025-02760-w> (2025).
20. Menoni, S. Chains of damages and failures in a metropolitan environment: some observations on the Kobe earthquake in 1995. *J. Hazard. Mater.* **86**(1), 101–119. [https://doi.org/10.1016/s0304-3894\(01\)00257-6](https://doi.org/10.1016/s0304-3894(01)00257-6) (2001).
21. Peijun, S. Theory and practice on disaster system research in a fifth time. *J. Nat. Disast.* **18**(05), 1–9. <https://doi.org/10.3969/j.issn.1004-4574.2009.05.001> (2009).

22. Shuai Min;Guo Haixiang;Liu Xiao;Wang Deyun;Chen Weiming. Inference Model of Rainstorm-Geology and Rainstorm-Flood Disaster Chain Based on Bayesian Network. *Science and Technology Management Research* **41**(04), (2021).
23. Standard of Classification for Geological Hazard:T/CAGHP 001-2018 (2018).
24. Swanson, J. Business dynamics: Systems thinking and modeling for a complex world. *The J. Operat. Res. Soc.* **53**(4), 472–473. <https://doi.org/10.1057/palgrave.jors.2601336> (2002).
25. Yao, T., Lijuan, W., Ziyang, T. & Lisheng, Li. Disaster analysis of “8·20” Wenchuan rainstorm disaster chain based on “Gaofen + emergency monitoring”. *Land and Resour. Inform.* **03**, 22–27 (2020).
26. Thapa, S. et al. Sediment transport and flood risk: impact of newly constructed embankments on river morphology and flood dynamics in Kathmandu Nepal. *Water Resour. Res.* **60**(10), 2024WR7742. <https://doi.org/10.1029/2024wr037742> (2024).
27. Wang, Yu, & Jinli, G. Evaluation method of node importance in directed-weighted complex network based on multiple influence matrix. *Acta Phys. Sinica* **66**(05), 19–30 (2017).
28. Zongzhi, Wu, & Mao, L. Gradation and categorization system of emergency plan for major accidents and their main contents. *Chin. Safety Sci. J.* **01**, 18–21 (2003).
29. Yang Qigui, Zhou Heqing. Category division of barrier lake and consideration on safety standard. *Yangtze River* **39** (22) (2008).
30. Yang, Y. et al. Susceptibility risk assessment of oil and gas pipeline geological hazards in mountainous areas based on data-driven model. *Eng. Appl. Artific. Intell.* **151**, 110732. <https://doi.org/10.1016/j.engappai.2025.110732> (2025).
31. Zening, W. et al. Assessing urban flood disaster risk using Bayesian network model and GIS applications. *Geomatic., Nat. Hazard. Risk* **10**(1), 2163–2184. <https://doi.org/10.1080/19475705.2019.1685010> (2019).
32. Kun, Z., Qibai, Li, & Baoping, Z. Evaluation Method for Node Importance in Directed-Weighted Complex Networks Based on PageRank. *J. Nanjing Univ. Aeronautics & Astronautics* **45**(03), 429–434. <https://doi.org/10.16356/j.1005-2615.2013.03.001> (2013).
33. Axing, Z. & Zongjin, Ma. Appraising study for the loss evaluation system of natural disasters. *J. Nat. Disast.* **03**, 1–7 (1993).
34. Zhou Sen. Risk Analysis of the Karst Collapse in Guangzhou Baiyun District Based on Analytical Hierarchy Process Combined with with Probability Calculation [Master's thesis]. South China University of Technology (2013).

Author contributions

P. had the original idea for the study, was responsible for data collecting, and wrote the first draft. D. was responsible for providing theoretical support and revising the paper. C. conducted the data analysis. All authors read and approved the final manuscript.

Funding

No funding.

Declarations

Competing interests

The authors declare no competing interests.

Additional information

Correspondence and requests for materials should be addressed to C.D.

Reprints and permissions information is available at www.nature.com/reprints.

Publisher's note Springer Nature remains neutral with regard to jurisdictional claims in published maps and institutional affiliations.

Open Access This article is licensed under a Creative Commons Attribution-NonCommercial-NoDerivatives 4.0 International License, which permits any non-commercial use, sharing, distribution and reproduction in any medium or format, as long as you give appropriate credit to the original author(s) and the source, provide a link to the Creative Commons licence, and indicate if you modified the licensed material. You do not have permission under this licence to share adapted material derived from this article or parts of it. The images or other third party material in this article are included in the article's Creative Commons licence, unless indicated otherwise in a credit line to the material. If material is not included in the article's Creative Commons licence and your intended use is not permitted by statutory regulation or exceeds the permitted use, you will need to obtain permission directly from the copyright holder. To view a copy of this licence, visit <http://creativecommons.org/licenses/by-nc-nd/4.0/>.

© The Author(s) 2026